Influence of s and d Orbital Occupation on the Binding of Metal Ions to Imidazole

N. S. Rannulu, R. Amunugama, Zhibo Yang, and M. T. Rodgers*

Department of Chemistry, Wayne State University, Detroit, Michigan 48202

Received: April 5, 2004; In Final Form: May 19, 2004

Threshold collision-induced dissociation of M^+(imidazole) with Xe is studied using guided ion beam mass spectrometry techniques. The metal ions, M^+, studied include: Na^+, Mg^+, Al^+, Ca^+, Sc^+, Ti^+, V^+, Cr^+, Mn^+, Fe^+, Co^+, Ni^+, Cu^+, and Zn^+. For the systems involving Na^+, Mg^+, Al^+, Ca^+, and the late transition metals, Cr^+ through Cu^+, the primary product corresponds to endothermic loss of the intact imidazole molecule. For the Zn^+ system, this process also occurs but forms Zn + imidazole$^+$ as the dominant product and Zn^+ + imidazole as a minor dissociation pathway. For the complexes to the early transition metal ions, Sc^+, Ti^+, and V^+, loss of the intact imidazole ligand competes with endothermic elimination of HCN to form M^+-(C_2H_3N). The energy-dependent collision-induced dissociation cross sections for M^+(imidazole) are modeled to yield threshold energies that are directly related to 0 and 298 K bond dissociation energies (BDEs) for M^+−imidazole after accounting for the effects of multiple ion-neutral collisions, kinetic and internal energy distributions of the reactants, and lifetimes for dissociation. Density functional theory calculations at the B3LYP/6-31G* level of theory are performed to determine the structures of these and the H^+, Li^+, and K^+ complexes and to provide molecular constants needed for the thermochemical analysis of experimental data. Theoretical BDEs are determined from single point energy calculations with an extended basis set, B3LYP/6-311+G(2d,2p), using the B3LYP/6-31G* optimized geometries. Excellent agreement between this level of theory and experiment is found for the Mn^+, Fe^+, Co^+, Ni^+, Cu^+, and Zn^+ systems examined here and for Li^+ and K^+ examined in earlier work. Although the agreement between theory and experiment is not as good for the other systems, the periodic trends in the BDEs are nearly parallel. Calculations at several other levels of theory are also performed to determine the level of theory required to obtain accurate energetics for these systems. The measured BDEs are compared to those previously measured for ammonia and adenine and to results for alkali metal ions bound to imidazole. The periodic trends are found to parallel those previously measured for these nitrogen donor ligands, suggesting that the binding in these complexes is very similar. The activated dissociation pathway observed in the complexes to the early transition metals also parallels that observed in complexes to adenine.

Introduction

Studies of the interactions between metal ions and small molecules of biological relevance in the gas phase have contributed useful insight into the properties of these interactions in the absence of solvation. In particular, studies directed toward an understanding of metal ion−nucleic acid and metal ion−protein interactions have seen a flurry of activity. Motivation for such studies comes from the fact that metal ions are ubiquitous in biological processes. The presence, identity, site of binding, and concentration of metal ions strongly influence the conformations of proteins and nucleic acids, which in turn control their activities. The effects of metal ion binding vary from stabilization of three-dimensional structure, catalysis of biochemical reactions, transport of substrate molecules, to transcription failure and even cell death.

Although metal ions are known to participate in biological processes,[1] the complexity of these systems makes it difficult to obtain detailed and systematic information on how the identity of the metal ion influences these functions. The specific metal ion identity is likely to be a crucial aspect in cases where metal ions play a direct role, as in oxidation−reduction reactions. In contrast, the size and charge of the metal ion may be the most influential factors when metal ions exert a more indirect influence, perhaps by inducing conformational changes. Alternatively, undesired effects can occur when the wrong metal ions are present, or even essential metal ions in the wrong concentrations.[2] For example, substitution of the native metal ion at the active site of an enzyme by another metal ion may alter the rate of, or completely shut down, the catalyzed biochemical reaction.

In trying to quantitatively assess such interactions in complex biological systems, a potentially useful first step is to measure the intrinsic binding energies of various metal ions to model systems. Alkali metal ions have a low tendency to form covalent bonds and are therefore less likely to exhibit strong specificity in their binding sites. In contrast, transition metal ions can form multiple covalent bonds and generally bind much more strongly to simple electron donors[3] (e.g., NH_3[4]) than the alkali metal ions, and are therefore likely to exhibit greater specificity in their binding.

In biological systems, alkali metal ions are found exclusively in the +1 charge state. In contrast, transition metal ions may occur in multiple oxidation states that include the +1 charge state for copper, cobalt, and nickel.[5] Further, free metal ions are not important reagents in biological systems; instead, they appear in a complex molecular scaffolding that orients ligands

* Corresponding author. Phone: (313)577-2431. E-mail: mrodgers@chem.wayne.edu.

10.1021/jp048500s CCC: $27.50
Published on Web 07/07/2004

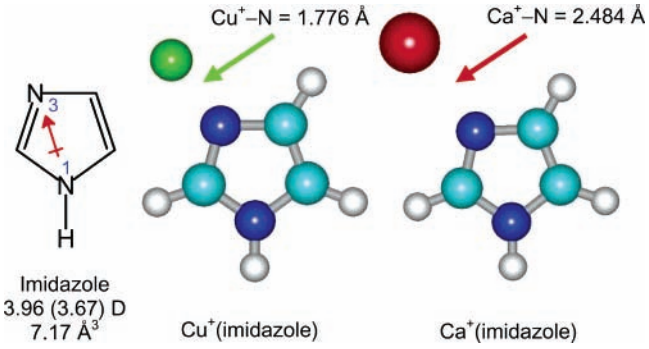

Figure 1. Structure of imidazole. The dipole moment in Debye is shown as an arrow and determined from theoretical calculations performed here; the measured dipole moment is given in parentheses.[24] The estimated polarizability is also shown.[25] Optimized B3LYP/6-31G* geometries of Cu^+(imidazole) and Ca^+(imidazole) showing the M^+-N bond distance for these structures.

to stabilize the metal ions, satisfy their electron deficiency, and permit them to undergo selective chemistry. However, in thinking about the thermodynamics of such species, it should be realized that a formal oxidation state is not equivalent to the real electron deficiency, precisely because the metal ions exist in a solvated or ligated environment where electron density is donated to the metal ion. Indeed, direct measurements of ligand binding affinities to multiply charged bare metal ions would be truly irrelevant to biological function because the increased electron deficiency would cause these metal ions to be much more reactive than when they are present in partially solvated or ligated environments. Therefore, the intrinsic bond energies and reactivities measured here for the +1 oxidation states may be useful analogues of the binding and reactivity of partially solvated metal ions in the +2 or +3 charge states, where the latter would be difficult to measure directly. Further, such intrinsic bond energies can be combined with solvation energies or the binding energies to other constituents of the biological system to allow a quantitative assessment of the competition among various possible binding sites. In addition, trends in the s and d orbital occupation, as explored in this work, should be largely independent of the charge and may provide insight into details of the binding mechanisms that should be useful in understanding a variety of real biochemical environments. Finally, such gas-phase thermochemistry can provide benchmarks for comparison to theory, which may then be used with more confidence on increasingly complex systems. Overall, the measurements described herein can be viewed as providing a useful "thermodynamic vocabulary" for thinking quantitatively about metal ion interactions with ligands of biological relevance.

In recent work, we have developed methods to allow the application of quantitative threshold collision-induced dissociation (CID) methods to obtain accurate thermodynamic information on increasingly large systems.[6−23] One of the driving forces behind these developments is our interest in applying such techniques to systems having biological relevance. In addition, we seek to perform accurate thermochemical measurements that provide absolute anchors for metal ion affinity scales over an ever-broadening range of energies.

In the present study, we examine the interactions of imidazole with a variety of metal ions. The structure of imidazole is shown in Figure 1 along with its calculated[19] and measured[24] dipole moments, and estimated polarizability.[25] Imidazole was chosen as a simple model of noncovalent interaction with metal ions for a wide variety of nitrogen-containing heterocycles of biological importance and, of particular interest, the nucleic acid bases and the amino acid histidine. In the present study, we use guided ion beam mass spectrometry to collisionally excite complexes of M^+ bound to imidazole, where $M^+ = Na^+$, Mg^+, Al^+, Ca^+, Sc^+, Ti^+, V^+, Cr^+, Mn^+, Fe^+, Co^+, Ni^+, Cu^+, and Zn^+. The kinetic energy-dependent cross sections for the CID processes are analyzed using methods developed previously.[8] The analysis explicitly includes the effects of the internal and translational energy distributions of the reactants, multiple collisions, and the lifetime for dissociation. We derive M^+-imidazole bond dissociation energies (BDEs) for all of the complexes except those for which $M^+ = Sc^+$, Ti^+, and V^+, where only upper and lower bounds for the BDEs are determined, and we compare these results to the theoretical values determined here and those in the literature.[3,11,19] We also compare the present results for imidazole to previous experimental results obtained for ammonia[4] and adenine[18] bound to these metal ions and to the results for alkali metal ions bound to imidazole.[9,19]

Experimental Section

General Procedures. A guided ion beam tandem mass spectrometer that has previously been described in detail[16] was used to measure absolute CID cross sections of M^+(imidazole) complexes. The M^+(imidazole) complexes are generated in a flow tube ion source by condensation of the metal ion and neutral imidazole molecule. These complexes are collisionally stabilized and thermalized by $>10^5$ collisions with the He and Ar bath gases such that ions emanating from the source region are well described by a Maxwell−Boltzmann distribution at room temperature. The ions are extracted from the source, accelerated, and focused into a magnetic sector momentum analyzer for mass analysis. Mass-selected ions are decelerated to a desired kinetic energy and focused into an octopole ion guide. The octopole passes through a static gas cell containing Xe at low pressures (0.05 and 0.20 mTorr), to ensure that multiple ion−neutral collisions are improbable. The octopole ion guide acts as an efficient trap for ions in the radial direction. Therefore, loss of scattered reactant and products ions in the octopole region is almost entirely eliminated.[26] Xe is used here, and in general for all of our CID measurements, because it is heavy and polarizable and therefore leads to more efficient kinetic to internal energy transfer in the CID process.[27−29] Product and unreacted beam ions drift to the end of the octopole where they are focused into a quadrupole mass filter for mass analysis and subsequently detected with a secondary electron scintillation detector and standard pulse counting techniques.

Ion intensities are converted to absolute cross sections using a Beers' law analysis as described previously.[30] Absolute uncertainties in the cross section magnitudes are estimated to be ±20%, which is largely the result of errors in the pressure measurement and length of the interaction region. Relative uncertainties are approximately ±5%.

Ion kinetic energies in the laboratory frame, E_{lab}, are converted to energies in the center of mass frame, E_{CM}, using the formula $E_{CM} = E_{lab}m/(m + M)$, where M and m are the masses of the ionic and neutral reactants, respectively. All energies reported here are in the CM frame unless otherwise noted. The absolute zero and distribution of the ion kinetic energies are determined using the octopole ion guide as a retarding potential analyzer as previously described.[30] The distribution of ion kinetic energies is nearly Gaussian with a fwhm between 0.3 and 0.7 (lab) for these experiments. The uncertainty in the absolute energy scale is ±0.05 eV (lab).

Pressure-dependent studies of all cross sections examined here were performed because multiple collisions can influence the

shape of CID cross sections and the threshold regions are most sensitive to these effects. Data free from pressure effects are obtained by extrapolating to zero reactant pressure, as described previously.[31] Thus, cross sections subjected to thermochemical analysis are the result of single bimolecular encounters.

Thermochemical Analysis. The threshold regions of the reaction cross sections are modeled using eq 1

$$\sigma(\mathrm{E}) = \sigma_0 \sum_i g_i(E + E_i - E_0)^n/E \qquad (1)$$

where σ_0 is an energy-independent scaling factor, E is the relative translational energy of the reactants, E_0 is the threshold for reaction of the ground electronic and ro-vibrational state, and n is an adjustable parameter that describes the efficiency of kinetic to internal energy transfer.[32] The summation is over the ro-vibrational states of the reactant ions, i, where E_i is the excitation energy of each state and g_i is the population of those states ($\sum g_i = 1$). The relative reactivity of all ro-vibrational states, as reflected by σ_0 and n, is assumed to be equivalent.

The density of the ro-vibrational states is determined using the Beyer−Swinehart algorithm,[33] and the relative populations, g_i, are calculated for a Maxwell−Boltzmann distribution at 298 K, the temperature appropriate for the reactants. The vibrational frequencies and rotational constants are derived from electronic structure calculations as described in the Theoretical Calculations section. The average vibrational energies at 298 K of the M^+(imidazole) complexes are given in Table 1S of the Supporting Information. We have increased and decreased the prescaled vibrational frequencies by 10% to encompass the range of average scaling factors needed to bring the calculated frequencies into agreement with experimentally determined frequencies as found by Pople et al.[34] The corresponding change in the average vibrational energy is taken to be an estimate of one standard deviation of the uncertainty in vibrational energy (Table 1S).

We also consider the possibility that collisionally activated ions do not dissociate on the time scale of our experiment (~100 μs) by including statistical theories for unimolecular dissociation, specifically Rice−Ramsperger−Kassel−Marcus (RRKM) theory, into eq 1 as described in detail elsewhere.[8,35] This requires sets of ro-vibrational frequencies appropriate for the energized molecules and the transition states (TSs) leading to dissociation. The former sets are given in Tables 1S and 2S, whereas we assume that the TSs are loose and product-like because the interaction between the metal ion and the imidazole molecule is largely electrostatic. In this case, the TS vibrations used are the frequencies corresponding to the products, which are also found in Table 1S. The transitional frequencies, those that become rotations and translations of the completely dissociated products, are treated as rotors, a treatment that corresponds to a phase space limit (PSL) and is described in detail elsewhere.[8]

The model represented by eq 1 is expected to be appropriate for translationally driven reactions[36] and has been found to reproduce CID cross sections well.[4,6−18,22,23,27−32] The model is convoluted with the kinetic energy distributions of both the reactant M^+(imidazole) complex and the neutral Xe atom, and a nonlinear least-squares analysis of the data is performed to give optimized values for the parameters σ_0, E_0, and n. The error associated with the measurement of E_0 is estimated from the range of threshold values determined for different zero-pressure extrapolated data sets, variations associated with uncertainties in the vibrational frequencies, and the error in the absolute energy scale, 0.05 eV (lab). For analyses that include RRKM lifetime effects, the uncertainties in the reported E_0 values also include the effects of increasing and decreasing the time assumed available for dissociation by a factor of 2.

Equation 1 explicitly includes the internal energy of the ion, E_i. All energy available is treated statistically because the ro-vibrational energy of the reactants is redistributed throughout the ion upon impact with the collision gas. The threshold for dissociation is by definition the minimum energy required leading to dissociation and thus corresponds to formation of products with no internal excitation. The threshold energies for dissociation reactions determined by analysis with eq 1 are converted to 0 K bond dissociation energies (BDEs) by assuming that E_0 represents the energy difference between reactants and products at 0 K.[37] This assumption requires that there are no activation barriers in excess of the endothermicity of dissociation, which should be valid for the simple electrostatic bond fission reactions examined here.[38]

Theoretical Calculations. To obtain model structures, vibrational frequencies, rotational constants, and energetics for the neutral imidazole ligand and for the M^+(imidazole) complexes, density functional calculations were performed using Gaussian 98.[39] Geometry optimizations and frequency analyses of the geometry optimized structures were performed at the B3LYP/6-31G* level.[40,41] In the calculations performed for all of the complexes, the spin state was assumed to be the same as the ground state for the bare metal ion (i.e., Li^+ singlet, Na^+ singlet, Mg^+ doublet, Al^+ singlet, K^+ singlet, Ca^+ doublet, Sc^+ triplet, Ti^+ quartet, V^+ quintet, Cr^+ sextet, Mn^+ septet, Co^+ triplet, Ni^+ doublet, Cu^+ singlet, and Zn^+ doublet), except for Fe^+ where calculations were performed for both the sextet ground state and the quartet first excited state. When used to model the data or to calculate thermal energy corrections, the B3LYP/6-31G* vibrational frequencies are scaled by a factor of 0.9804.[42] The scaled vibrational frequencies thus obtained for these systems are available as Supporting Information and are listed in Table 1S, while Table 2S lists the rotational constants. Single point energy calculations were performed at the B3LYP/6-311+G(2d,2p) level using the B3LYP/6-31G* optimized geometries. To obtain accurate BDEs, zero point energy (ZPE) corrections were applied and basis set superposition errors (BSSE) were subtracted from the computed dissociation energies in the full counterpoise approximation.[43,44]

In earlier work,[9,19] we investigated the interactions of the H^+, Li^+, Na^+, and K^+ with imidazole. In those studies, calculations were performed at the MP2(full)/6-311+G(2d,2p)//MP2(full)/6-31G* level of theory. Computations at this level of theory for the transition metal ions require more resources than are currently available to us, thus necessitating our choice of B3LYP calculations in the present work. To allow comparison of the theoretical results determined here to those in these earlier studies, we also performed B3LYP calculations for the complexes of imidazole to H^+, Li^+, and K^+. Likewise, we extended our MP2(full) calculations to include those computationally feasible: Mg^+, Al^+, Ca^+, Cu^+, and Zn^+. To test the accuracy of the B3LYP and MP2 results, we also carried out single point energy calculations at both levels of theory using an even larger basis set, 6-311++G(3df,3pd), and using complete basis set extrapolations at the CBS-Q and CBS-QB3 levels of theory for the complexes of imidazole to H^+, Li^+, Na^+, K^+, Mg^+, Al^+, Ca^+, Cu^+, and Zn^+.

Results

Cross Sections for Collision-Induced Dissociation. Experimental cross sections were obtained for the interaction of Xe

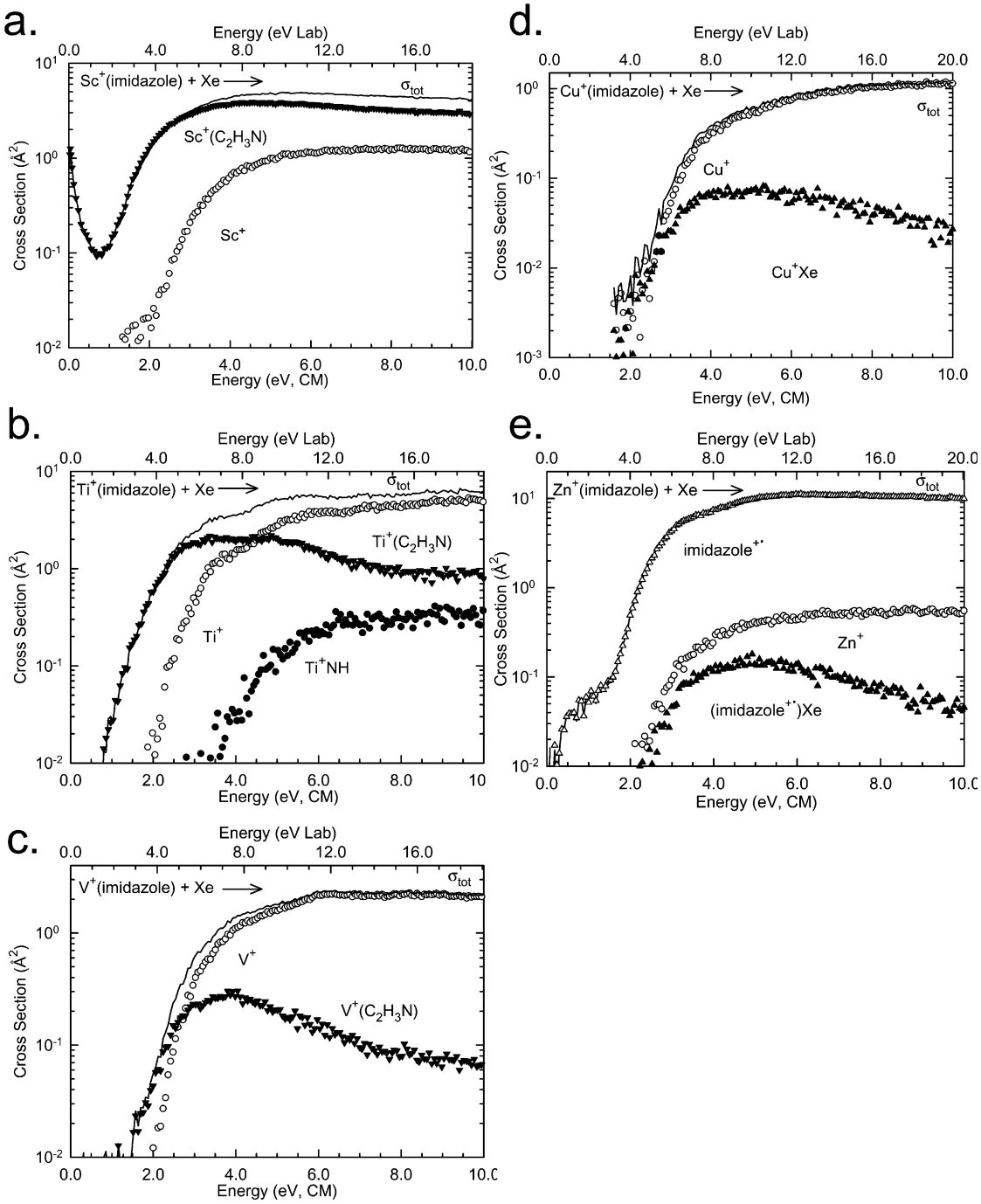

Figure 2. Cross sections for the collision-induced dissociation of the M^+(imidazole) complexes with Xe as a function of collision energy in the center-of-mass frame (lower *x*-axis) and laboratory frame (upper *x*-axis), where $M^+ = Sc^+$, Ti^+, V^+, Cu^+, and Zn^+, parts a−e, respectively. Cross sections for the M^+ CID product channel (○), imidazole$^{+\bullet}$ CID charge-transfer channel (△), $M^+(C_2H_3N)$ activated dissociation channel (▼), MNH^+ sequential activated dissociation channel (●), and M^+Xe ligand exchange channel (▲) are shown when observed.

with 14 M^+(imidazole) complexes, where $M^+ = Na^+$, Mg^+, Al^+, Ca^+, Sc^+, Ti^+, V^+, Cr^+, Mn^+, Fe^+, Co^+, Ni^+, Cu^+, and Zn^+. Figure 2 shows representative data for the Sc^+(imidazole), Ti^+(imidazole), V^+(imidazole), Cu^+(imidazole), and Zn^+-(imidazole) complexes. The other M^+(imidazole) complexes show relative behavior similar to that of the Cu^+(imidazole) complex. The most favorable process for most complexes is the loss of the intact imidazole molecule in the CID reactions 2.

$$M^+(\text{imidazole}) + Xe \rightarrow M^+ + \text{imidazole} + Xe \quad (2)$$

For Zn^+(imidazole), the same dissociation process occurs but is only a minor reaction pathway because the relative ionization energies of the fragments, IE(Zn) = 9.394 eV[45] and IE-(imidazole) = 8.81 ± 0.01 eV[46] are such that the dominant ionic product is now the imidazole ligand, reaction 3.

$$Zn^+(\text{imidazole}) + Xe \rightarrow Zn + \text{imidazole}^+ + Xe \quad (3)$$

The chemistry observed for the early transition metal systems, Sc^+(imidazole), Ti^+(imidazole), and V^+(imidazole), shows greater complexity, Figures 2a−c. An additional activated dissociation pathway is observed in all three systems corresponding to endothermic loss of HCN, reaction 4.

$$M^+(\text{imidazole}) + Xe \rightarrow M^+(C_2H_3N) + HCN + Xe \quad (4)$$

TABLE 1: Modeling Parameters of Eq 1 and Entropies of Activation at 1000 K of M^+(imidazole)[a]

reactant ion	ionic product	σ_0[b]	n[b]	E_0[c] (eV)	E_0(PSL) (eV)	kinetic shift (eV)	$\Delta S^{\ddagger}$(PSL) (J mol^{-1} K^{-1})
Na^+(imidazole)	Na^+	0.7 (0.1)	1.4 (0.1)	1.45 (0.07)	1.45 (0.05)	0.00	28 (2)
Mg^+(imidazole)	Mg^+	2.3 (0.3)	1.2 (0.1)	2.68 (0.11)	2.53 (0.11)	0.15	32 (2)
Al^+(imidazole)	Al^+	1.8 (0.1)	1.3 (0.1)	2.58 (0.06)	2.41 (0.07)	0.17	33 (2)
Ca^+(imidazole)	Ca^+	3.3 (0.2)	1.0 (0.1)	1.95 (0.03)	1.93 (0.04)	0.02	27 (2)
Sc^+(imidazole)	Sc^+	1.5 (0.2)	1.2 (0.1)	$\leq$3.09 (0.09)	$\leq$2.83 (0.09)	0.26	28 (2)
Sc^+(imidazole)[d]	σ_{tot}	1.7 (0.1)	1.5 (0.1)	$\geq$1.96 (0.06)	$\geq$1.94 (0.04)	0.02	30 (2)
Ti^+(imidazole)	Ti^+	2.2 (0.2)	1.6 (0.1)	$\leq$2.50 (0.04)	$\leq$2.41 (0.02)	0.09	33 (2)
Ti^+(imidazole)[d]	σ_{tot}	3.5 (0.2)	1.4 (0.1)	$\geq$1.83 (0.03)	$\geq$1.82 (0.01)	0.01	34 (2)
V^+(imidazole)	V^+	1.6 (0.1)	1.3 (0.1)	$\leq$2.63 (0.09)	$\leq$2.52 (0.07)	0.11	35 (2)
V^+(imidazole)	σ_{tot}	1.9 (0.1)	1.2 (0.1)	$\geq$2.35 (0.04)	$\geq$2.29 (0.02)	0.06	35 (2)
Cr^+(imidazole)	Cr^+	2.3 (0.2)	1.2 (0.1)	2.35 (0.05)	2.28 (0.03)	0.07	36 (2)
Mn^+(imidazole)	Mn^+	2.1 (0.3)	1.2 (0.1)	2.30 (0.05)	2.22 (0.03)	0.08	30 (2)
Fe^+(imidazole)	Fe^+	3.3 (0.3)	1.5 (0.5)	2.69 (0.14)	2.55 (0.01)	0.14	36 (2)
Co^+(imidazole)	Co^+	1.2 (0.2)	1.3 (0.1)	2.97 (0.13)	2.79 (0.09)	0.18	39 (2)
Ni^+(imidazole)	Ni^+	1.8 (0.4)	2.1 (0.1)	2.82 (0.06)	2.66 (0.08)	0.16	41 (2)
Cu^+(imidazole)	Cu^+	1.1 (0.1)	1.1 (0.1)	3.22 (0.06)	2.98 (0.03)	0.24	41 (2)
Zn^+(imidazole)[e]	imidazole$^+$	14.4 (2.1)	1.1 (0.1)	2.30 (0.03)	2.24 (0.04)	0.06	37 (2)
	Zn^+	0.7 (0.1)	1.2 (0.1)	2.76 (0.04)	2.62 (0.10)	0.14	36 (2)
Zn^+(imidazole)[f]	imidazole$^+$	7.2 (0.9)	1.2 (0.1)		2.21 (0.03)		39 (2)
	Zn^+				2.36 (0.04)		37 (2)

[a] Uncertainties are listed in parentheses. [b] Average values for loose PSL transition state. [c] No RRKM analysis. [d] Values obtained for fits to the total cross section. [e] Values obtained for independent fits to the reaction channels. [f] Values obtained for competitive fits to the reaction channels.

Reaction 4 is the dominant low energy process for all three metal ions. The cross section for reaction 4 decreases at elevated energies as a result of competition with reaction 2, the entropically favored pathway. Our experiments do not provide sufficient information to determine the structure of the M^+-(C_2H_3N) product, but it seems likely that upon activated dissociation the complex rearranges to $M^+(N{\equiv}CCH_3)$ such that the metal ion is bound to acetonitrile. This activated dissociation process is most favorable for Sc^+ and is the dominant reaction pathway at all energies. Two features are observed in this product cross section. At low energies, the cross section decreases with increasing energy, indicating a minor exothermic reaction pathway, and then at ~0.8 eV begins increasing with increasing energy, indicating a major endothermic reaction pathway for this activated dissociation process. The analogous process becomes increasingly less favorable for the Ti^+ and V^+ systems, respectively. Neither system exhibits behavior indicative of an exothermic reaction pathway. The magnitudes of the cross sections for this activated dissociation process decrease, while the apparent thresholds increase from Sc^+ to Ti^+ to V^+. An additional minor reaction pathway is also observed only in the Ti^+ system. The cross section for the $Ti^+(C_2H_3N)$ product falls off as this additional product, $TiNH^+$, grows in. The energy dependence of the cross sections for these products indicates that $TiNH^+$ is formed sequentially via endothermic loss of $HC{\equiv}CH$ from $Ti^+(C_2H_3N)$ rather than directly from the reactant Ti^+(imidazole) complex, reaction 5.

$$Ti^+(C_2H_3N) \rightarrow TiNH^+ + HC{\equiv}CH \qquad (5)$$

The only other product that is observed in the CID of the M^+-(imidazole) complexes with Xe is the result of a ligand exchange process to form MXe^+. The cross sections for the MXe^+ products are approximately 1−2 orders of magnitude smaller than those of M^+, the primary dissociation product. The MXe^+ ligand exchange product is observed only in the Na^+, Al^+, Cr^+, Co^+, Ni^+, and Cu^+ systems. The ligand exchange reaction pathway probably exists with similar probability for all complexes; its absence in the other systems most likely occurs as a result of weaker reactant ion beam intensities for those systems.

Theoretical Results. Structures for neutral imidazole and for the complexes of imidazole to H^+, Li^+, Na^+, Mg^+, Al^+, K^+, Ca^+, Sc^+, Ti^+, V^+, Cr^+, Mn^+, Fe^+, Co^+, Ni^+, Cu^+, and Zn^+ were calculated as described in the Theoretical Calculations section. Table 3S in the Supporting Information gives details of the optimized structures for each of these species. As for the alkali metal ion complexes, binding of the metal ion at the N3 site is preferred over the N1 site and the π cloud of the aromatic ring. The distortion of the imidazole molecule that occurs upon complexation is minor, Table 3S. The primary difference in the structure of these complexes corresponds to the M^+−N bond distance. Of the complexes examined both experimentally and theoretically in this work, Cu^+ is found to have the shortest metal−ligand bond distance, 1.776 Å, while Ca^+ is found to have the longest, 2.484 Å. The optimized structures of the M^+-(imidazole) complexes to these two metal ions are shown in Figure 1. The calculated enthalpies of proton and metal ion binding to imidazole determined at several levels of theory (B3LYP/6-311+G(2d,2p) ≡ B3LYP, B3LYP/6-311++G(3df,-3pd) ≡ B3LYPext, MP2(full)/6-311+G(2d,2p) ≡ MP2(full), MP2(full)/6-311++G(3df,3pd) ≡ MP2(full)ext, CBS-Q, and CBS-QB3) are summarized in Table 2 along with MP2 values reported earlier.[19]

Threshold Analysis. The model of eq 1 was used to analyze the thresholds for reaction 2 in all 14 M^+(imidazole) systems and reaction 3 in the Zn^+(imidazole) system. In addition, reactions 2 and 3 in the Zn^+(imidazole) system were modeled simultaneously using a competitive analysis described in detail previously.[15] The total cross sections in the M^+(imidazole) systems, where $M^+ = Sc^+$, Ti^+, and V^+, were also analyzed using the model of eq 1. The presence of the low-energy feature in the Sc^+(imidazole) system complicates the data analysis and was therefore subtracted from the total cross section before analysis. The results of these analyses are provided in Table 1, and representative analyses are shown in Figure 3 for the Cu^+(imidazole) and Zn^+(imidazole) complexes. The other systems exhibit comparable results and are shown as Figures 2S and 3S in the Supporting Information. In all cases, the experimental cross sections for reaction 2, reaction 3, and the total cross section are accurately reproduced using a loose PSL TS model.[8] Previous work has shown that this model provides the most accurate assessment of the kinetic shifts for CID processes for electrostatically bound ion−molecule com-

TABLE 2: Experimental and Calculated Enthalpies of Proton and Metal Ion Binding to Imidazole at 0 K in kJ/mol

	experiment		theory					
	GIBMS[a]	literature[b]	B3LYP[a,c] $D_{0,BSSE}$	B3LYPext[a,d] $D_{0,BSSE}$	MP2(full)[a,e] $D_{0,BSSE}$	MP2(full)ext[a,f] $D_{0,BSSE}$	CBS-Q D_0	CBS-QB3 D_0
H^+		936.6 (16.0)[g]	940.2	942.9	922.2[h]	941.3	936.3	936.5
Li^+	210.8 (9.5)[i]	187.6 (9.5)[j]	211.9	213.3	202.7[h]	220.1	204.6	204.0
Na^+	139.4 (6.4)		151.5	153.2	144.5[h]	163.8	146.8	140.6
	139.7 (5.2)[i]							
Mg^+	243.9 (10.4)		216.3	218.8	212.8	232.2	223.3	222.5
Al^+	232.4 (8.2)		205.2	209.3	204.5	227.7	223.4	221.9
K^+	109.0 (5.6)[i]		108.4	109.4	108.6[h]	127.6	97.8	94.9
Ca^+	186.3 (3.9)		174.2	179.9	165.7	188.0	156.2	145.7
Sc^+	≥186.7 (5.1)		244.7					
	≤272.8 (8.8)							
Ti^+	≥175.5 (2.6)		243.1					
	≤232.4 (8.2)							
V^+	≥221.2 (4.6)		254.1					
	≤243.4 (8.0)							
Cr^+	219.8 (5.5)		238.6					
Mn^+	214.2 (4.4)		209.7					
Fe^+	246.1 (13.8		245.0[k]					
			270.9[l]					
Co^+	268.8 (10.7)		271.2					
Ni^+	283.8 (9.4)		286.7					
Cu^+	287.5 (7.4)		284.9	287.8	275.8	301.7	261.3	284.1
Zn^+	252.5 (9.7)[m]		252.4	251.2	249.1	270.9	266.6	262.0
	216.1 (3.9)[n]		184.2	187.5	236.3	266.0	220.7	224.4

[a] This work except as noted. [b] All literature values adjusted to 0 K. [c] B3LYP/6-311+G(2d,2p)//B3LYP/6-31G*. [d] B3LYP/6-311++G(3df,3pd)//B3LYP/6-31G*. [e] MP2(full)/6-311+G(2d,2p)//MP2(full)/6-31G*. [f] MP2(full)/6-311++G(3df,3pd)//MP2(full)/6-31G*. [g] Reference 50. [h] Reference 19. [i] Reference 9. [j] Reference 51. [k] $Fe^+(s^1d^6, 6D)$. [l] $Fe^+(d^7, {}^4F)$. [m] Values for the Zn^+ + imidazole asymptote. [n] Values for the Zn + imidazole$^+$ asymptote.

plexes.[4,6−18,22,23] Good reproduction of the CID data is obtained over energy ranges exceeding 3.5 eV and cross-section magnitudes of at least a factor of 100. Table 1 also includes values of E_0 obtained without including the RRKM lifetime analysis. Comparison of these E_0 values with the E_0(PSL) values shows that the kinetic shifts observed for most of these systems are fairly small and vary between 0.02 and 0.26 eV, while the Na^+ systems exhibits no kinetic shift. The total number of vibrations, 24, and heavy atoms, 6, remains the same in all of the M^+(imidazole) complexes, and hence the number of low frequency vibrations remains the same. This implies that the observed kinetic shift should directly correlate with the density of states of the complex at threshold, which depends on the measured BDE. This is exactly what is found, as shown in Table 1.

In the Zn^+(imidazole) system, competition among reactions 2 and 3 is clearly occurring and might be expected to influence the threshold determinations. Conservatively, the threshold determined for reaction 2 without explicit consideration of this competition is an upper limit to the Zn^+−imidazole BDE. Indeed, competitve modeling of these reaction pathways influences the threshold determined for reaction 3 very little, by <0.03 eV, whereas the threshold determined for reaction 2 decreases by 0.26 eV.[15] The relative thresholds for these processes are expected to be determined by the difference in the ionization energies (IEs) of Zn, 9.39405 ± 0.00006 eV,[45] and imidazole, 8.81 ± 0.01 eV.[46] Assuming that the reported values for the IEs of Zn and imidazole are reliable, the measured thresholds should differ by 0.58 eV. Certainly, the IE of Zn is expected to be very reliable. However, four values have actually been reported for the IE of imidazole. The value mentioned above was determined by photoionization mass spectrometry measurements[46] and is believed to be the most reliable. There have also been two determinations of the vertical IE from photoelectron spectroscopy studies providing values of 8.78[47] and 8.96 eV.[48] Electron impact techniques, which are not expected to be as reliable as the other techniques, have also been used to determine the IE of imidazole and find a value of 9.12 eV.[49] If these values for the IE of imidazole are used, then the measured thresholds should differ by between 0.27 and 0.61 eV, but should more likely be at the high end of this range. Independent fitting of these reaction channels results in thresholds that differ by 0.38 eV, whereas competitive modeling results in thresholds that differ by only 0.15 eV. The competitive model used was originally developed to deal with ro-vibrational effects. This model may not be appropriate for modeling the electronic competition occurring in this system because electron motion is very rapid as compared to nuclear motions. This suggests that little or no effect on the threshold for these processes may result from this competition and that independent modeling may provide more reliable results. In any event, the relative thresholds determined from independent modeling of these reaction channels should reflect either the true difference or an upper limit for the difference in the IEs for Zn and imidazole. The relative thresholds determined here therefore suggest that the IE of imidazole is larger than the currently accepted value of 8.81 ± 0.01 eV. Because of the uncertainly in the appropriateness of the competitive model for dealing with electronic effects occurring in this system, the values reported for the Zn + imidazole$^+$ and the Zn^+ + imidazole product asymptotes will make use of the values determined from independent modeling of these two reaction channels.

In the case of the M^+(imidazole) systems where $M^+ = Sc^+$, Ti^+, and V^+, competition among reactions 2 and 4 is clearly occurring and certainly influences the threshold determinations. Unfortunately, explicit modeling of the competition requires knowledge of the transition states for reaction 4, which are likely to be tight transition states. Conservative upper and lower limits for the M^+−imidazole BDE are determined by analyzing the total CID cross section and the cross section for reaction 2 (while ignoring the effects of competition with reaction 4), respectively.

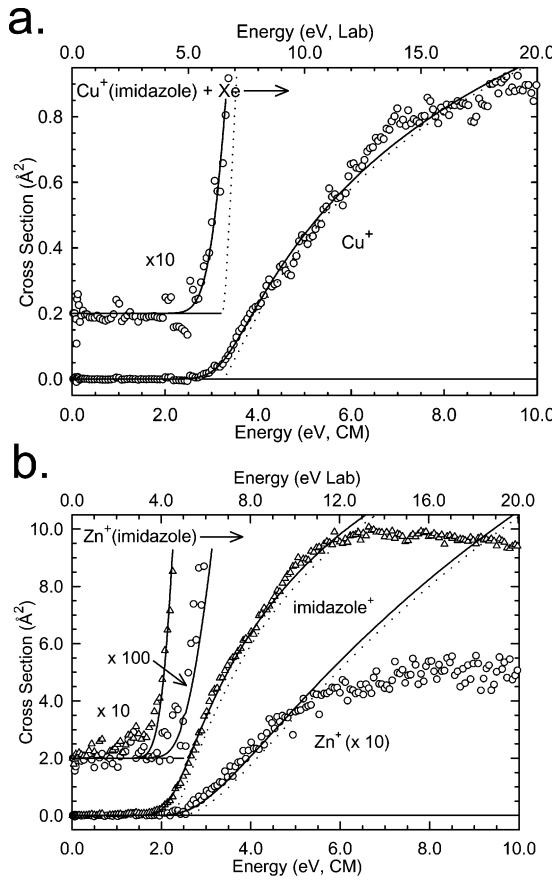

Figure 3. Zero-pressure-extrapolated cross section for collision-induced dissociation of M^+(imidazole) complexes with Xe in the threshold region as a function of kinetic energy in the center-of-mass frame (lower *x*-axis) and laboratory frame (upper *x*-axis), where $M^+ = Cu^+$ and Zn^+, parts a and b, respectively. The solid line shows the best fit to the data using eq 1 convoluted over the neutral and ion kinetic and internal energy distributions. The dotted line shows the model cross sections in the absence of experimental kinetic energy broadening for reactants with an internal energy corresponding to 0 K.

The entropy of activation, $\Delta S^{\ddagger}$, is a measure of the looseness of the TS and also a reflection of the complexity of the system. It is largely determined by the molecular parameters used to model the energized molecule and the TS for dissociation, but also depends on the threshold energy. Listed in Table 1, $\Delta S^{\ddagger}$(PSL) values at 1000 K show little variation, as expected based upon the similarity of these systems, and range between 27 and 41 J mol^{-1} K^{-1} across these systems. These entropies of activation are consistent with $\Delta S_{1000}^{\ddagger}$ values collected by Lifshitz for several simple bond cleavage dissociations of ions[50] as well as numerous systems previously studied in our laboratory.

Conversion from 0 to 298 K. To allow comparison to commonly employed experimental conditions, we convert the 0 K bond energies determined here to 298 K bond enthalpies and free energies. The enthalpy and entropy conversions are calculated using standard formulas (assuming harmonic oscillator and rigid rotor models) and the vibrational and rotational constants determined for the B3LYP/6-31G* optimized geometries; these are given in Tables 1S and 2S. Table 4S lists 0 and 298 K enthalpy, free energy, and enthalpic and entropic corrections for all systems experimentally determined (from Table 1) except for the complexes to Sc^+, Ti^+, and V^+ where only upper and lower bounds for the BDEs were determined. Uncertainties in the thermal corrections are determined by 10% variation in the vibrational frequencies. Because the M^+−imidazole frequencies are very low and may not be adequately described by theory, the listed uncertainties also include increasing and decreasing the three metal−ligand frequencies by a factor of 2. The latter provides a conservative estimate of computational errors in these low-frequency modes and is the dominant source of the uncertainties listed.

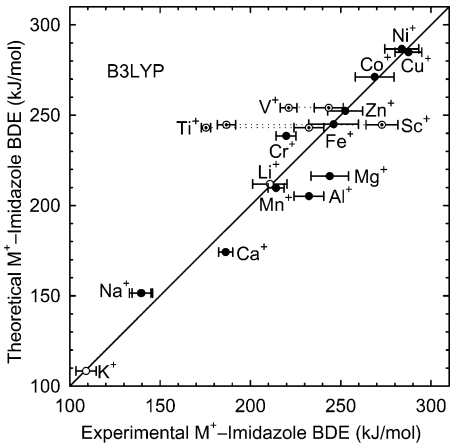

Figure 4. Theoretical versus experimental BDEs (in kJ/mol) of M^+−imidazole, where $M^+ = Li^+$, Na^+, Mg^+, Al^+, K^+, Ca^+, Sc^+, Ti^+, V^+, Cr^+, Mn^+, Fe^+, Co^+, Ni^+, Cu^+ and Zn^+. All values are at 0 K and taken from Table 2. Experimental results include estimated upper and lower bounds for the BDEs of the complexes to Sc^+, Ti^+, and V^+ (⊙); values for the alkali metal ions taken from ref 9 (○). The diagonal line indicates the values for which calculated and measured BDEs are equal.

Discussion

Comparison of Theory and Experiment. The M^+−imidazole BDEs at 0 K measured here by guided ion beam mass spectrometry are summarized in Table 2. Also listed here are the 0 K proton and metal ion binding energies calculated at various levels of theory, B3LYP, B3LYPext, MP2(full), and MP2(full)ext, all of which include ZPE and BSSE corrections,[51,52] and using complete basis set extrapolations at the CBS-Q and CBS-QB3 levels of theory. Experimental values for proton and alkali metal ion binding to imidazole taken from previous studies are also provided in Table 2 for comparison.[19,53,54] The agreement between the B3LYP and measured BDEs for the alkali metal ions, as well as the metal ions examined, here is illustrated in Figure 4. It can be seen that the agreement between theory and experiment is reasonable over the 180 kJ/mol variation in the measured BDEs. However, the theoretical value for the Na^+(imidazole) complex is higher than the measured values by ~12 kJ/mol, a larger discrepancy than is typical for Na^+(ligand) complexes.[11] In contrast, the theoretical values for Mg^+, Al^+, and Ca^+ are systematically lower than the measured values, again with larger discrepancies than might be expected for this level of theory. It is these discrepancies that led us to extend our calculations to several additional levels of theory for the computationally feasible systems.

For the 13 M^+(imidazole) systems for which absolute BDEs could be determined, the mean absolute deviation (MAD) between experiment and B3LYP theory is 8.7 ± 10.0 kJ/mol. This is similar to the average experimental error (AEE) in these values, 8.1 ± 2.9 kJ/mol. When the alkali metal ions are not included, the MAD is slightly larger, 9.9 ± 10.8 kJ/mol, while the AEE changes very little, 8.3 ± 3.1 kJ/mol. The MAD for the alkali metal ions is somewhat smaller, 4.6 ± 6.5 kJ/mol, and smaller than the AEE in these values, 7.2 ± 2.1 kJ/mol. When Na^+, Mg^+, Al^+, and Ca^+ are not included, the MAD falls to 3.8 ± 5.8 kJ/mol, while the AEE decreases slightly to

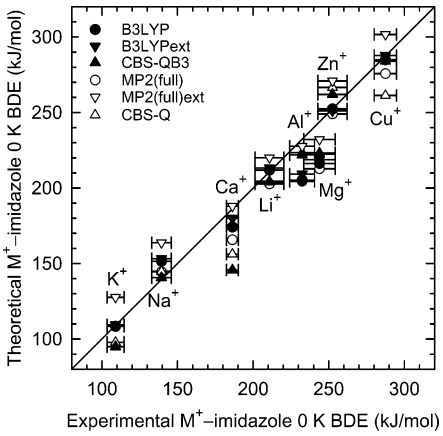

Figure 5. Theoretical versus experimental BDEs (in kJ/mol) of M^+−imidazole, where $M^+ = Li^+$, Na^+, Mg^+, Al^+, K^+, Ca^+, Cu^+, and Zn^+. All values are at 0 K and taken from Table 2. Calculated values are shown for the B3LYP (●), B3LYPext (▼), CBS-QB3 (▲), MP2(full) (○), MP2(full)ext (▽), and CBS-Q (△) levels of theory.

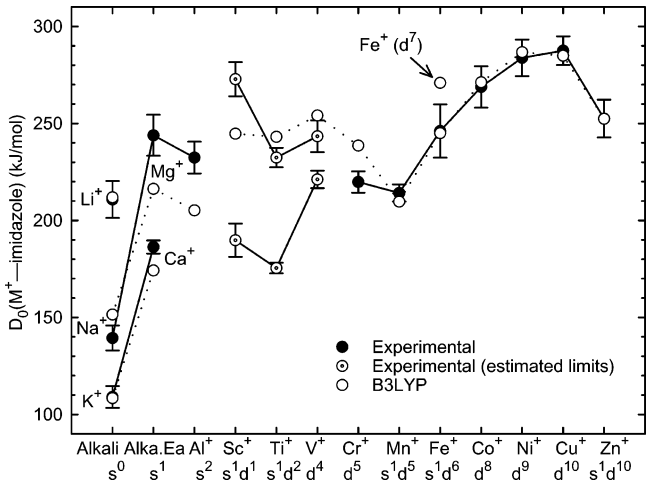

Figure 6. Periodic trends in M^+−imidazole BDEs (in kJ/mol), $M^+ = Li^+$, Na^+, Mg^+, Al^+, K^+, Ca^+, Sc^+, Ti^+, V^+, Cr^+, Mn^+, Fe^+, Co^+, Ni^+, Cu^+ and Zn^+. All values are at 0 K and taken from Table 2. Absolute experimental BDEs (●), estimated upper and lower bounds for the BDEs (⊙), and B3LYP values (○).

8.2 ± 2.9 kJ/mol. In this case, the primary contributor to the MAD is the Cr^+ system. Excluding this value, the MAD becomes much smaller, 2.2 ± 1.4 kJ/mol, while the AEE changes very little, 8.4 ± 3.1 kJ/mol. To determine the source of this inconsistency between experiment and theory, we repeated the experiments for these systems (Na^+, Mg^+, Al^+, Ca^+, and Cr^+) at least several times, but the measured BDEs were consistent in each determination. Therefore, we decided to pursue additional calculations using extended basis sets and complete basis set extrapolation techniques to determine if another level of theory was more suitable for accurate determination of the M^+−imidazole BDEs. As discussed above, these calculations require significantly more time and computational resources and were therefore limited to the complexes to H^+, Li^+, Na^+, Mg^+, Al^+, K^+, Ca^+, Cu^+, and Zn^+.

In the case of the protonated complexes, all six levels of theory are consistent with the measured proton affinity of imidazole and associated error in this measurement. However, both B3LYP BDEs are slightly high, the MP2 BDEs straddle the measured value with the 6-311+G(2d,2p) value exhibiting the poorest agreement, and the CBS-Q and CBS-QB3 BDEs are both in excellent agreement with the measured proton affinity. For the complexes to the metal ions, the results are not as consistent or quite as satisfying. The agreement between the various levels of theory and experiment for the eight M^+-(imidazole) systems is illustrated in Figure 5. The MADs between theory and experiment for these eight systems do not differ very much with the level of theory employed even though the calculated BDEs change markedly in many cases. The MADS are as follows: B3LYP, 10.4 ± 11.5 kJ/mol, B3LYPext, 9.1 ± 10.3 kJ/mol, MP2(full), 13.5 ± 11.6 kJ/mol, MP2(full)-ext, 12.9 ± 7.6 kJ/mol, CBS-Q, 15.6 ± 9.0 kJ/mol, and CBS-QB3, 13.4 ± 12.7 kJ/mol. In every case, the MADs are larger than the AEE of 7.6 ± 2.2 kJ/mol. This suggests that in general theory has difficulties properly handling the imidazole ligand. Indeed, G2 theory finds a BDE for the Na^+(imidazole) complex of 119.6 kJ/mol, an even poorer estimate of the binding energy than any of the levels of theory examined here.[11]

A more detailed examination of the agreement between the measured and calculated values shows that, in each case, typically only a few systems contribute to the large MADs. B3LYP appears to do a good job for most systems including the transition metal ions. The addition of more diffuse and polarization functions generally produces a small increase in the calculated M^+−imidazole BDEs, but leads to better agreement between theory and experiment for only half of the systems examined. The MP2(full) values appear to be low for all but the Na^+ and K^+ systems. The addition of more diffuse and polarization functions generally leads to a large increase in the M^+−imidazole BDEs, but also leads to better agreement between theory and experiment for only half of the systems examined. The complete basis set extrapolation protocols seem to suffer similar problems, providing better agreement in some cases, and poorer agreement in others. The CBS-QB3 protocol exhibits slightly better agreement with experiment than does the CBS-Q protocol, but both do a very poor job for K^+ and Ca^+. Based upon the results of this study, it is not clear which level of theory should be recommended as each suffers problems for at least a few metal ions. However, the B3LYP and B3LYPext levels of theory perform slightly better than the other levels of theory examined. It seems obvious that the imidazole ligand is problematic and a perfect example of why theory in the absence of experimental measurements cannot always be relied on to provide accurate thermochemistry.

Periodic Trends in the Binding of Metal Ions to Imidazole. The periodic trends in the measured M^+−imidazole BDEs determined here and those from previous studies[9,19] are illustrated in Figure 6. The theoretical BDEs are also shown, but limited to the B3LYP values for simplicity. As can be seen in the figure, the strength of the M^+−imidazole interaction is strongly dependent upon the size and electronic structure of the metal ion.

In earlier work, the interaction of imidazole with the alkali metal ions was examined.[9,19] As has been observed for a wide variety of ligands, the bond energy decreases from Li^+ to Na^+ to K^+. This is the expected trend for simple electrostatic binding. The alkali metal ions have an s^0 valence electron configuration, and thus their electron densities are spherically symmetric. The metal−ligand bond length is determined primarily by the size of the ion such that the smallest alkali metal ion, Li^+, exhibits the shortest metal−ligand bond distance and therefore the strongest electrostatic interaction. The metal−ligand bond distance increases from Li^+ to Na^+ to K^+, leading to a progressively weaker binding interaction.

The presence of a varying number of valence electrons in the other monocations examined in this work leads to more complicated interactions with imidazole than observed for the alkali metal ions. Systematic evaluation of the influence of the

valence electronic structure of the metal ion is therefore possible by examining the trends in the measured M^+−imidazole BDEs. The strength of the M^+−imidazole interaction is controlled by the balance of the ion-dipole electrostatic attraction, ion-induced dipole polarization attraction, and Pauli repulsion between the valence electrons of the metal ion and those donated by imidazole. The covalent nature of the M^+−imidazole interaction may be enhanced by charge transfer between the metal ion and the imidazole ligand, via ligand-to-metal donation and/or metal-to-ligand back-donation. Retention of electron density by each leads to bonding with greater ionic character. The imidazole ligand has three types of orbitals that can contribute to the binding. The N3 nitrogen lone pair is the primary donor of electron density, the occupied π orbitals of the aromatic ring may also act as donors of electron density, and the unoccupied π^* antibonding orbitals may act as acceptors of electron density.

s Orbital Occupation. The series of ions, Na^+ (and K^+), Mg^+ (and Ca^+), and Al^+ having valence electron configurations of s^0, s^1, and s^2 occupations, respectively, allow examination of the influence of s orbital occupation upon the strength of the binding energy. Pauli repulsion between the electron(s) on the metal ion and the nitrogen lone pair increases as the occupation of the s orbital increases. Therefore, in the absence of other factors, it would be expected that the bond energies would also decrease with increasing s orbital occupation. In contrast, the bond energies are observed to increase from Na^+ to Mg^+ and then to decrease somewhat for Al^+, although it is still significantly more strongly bound than Na^+. Similarly, the bond energy increases from K^+ to Ca^+. The enhancement in the bonding in the Mg^+ and Al^+ systems arises from 3s−3p hybridization,[55,56] while the enhancement in the bonding in the Ca^+ system arises from 4s−4p hybridization. Hybridization of the s and p orbitals requires energy, but creates two new orbitals, an occupied orbital oriented 180° away from the imidazole ligand and an empty orbital pointing at the imidazole ligand for donation by the nitrogen lone pair. Such hybridization provides a stronger electrostatic interaction by exposing a higher nuclear charge to imidazole. In the limit of complete removal of the valence electrons, this would correspond to binding to Mg^{2+}, Ca^{2+}, and Al^{3+}. Less enhancement of the binding in the Al^+ system as compared to the Mg^+ system is observed because electron removal is not complete, two electrons must be hybridized, and s−p hybridization requires more energy for Al^+ than for Mg^+. In both an absolute and a relative sense, less enhancement in the BDE on going from K^+ to Ca^+ is observed as compared to that measured for the Na^+ and Mg^+ systems. This is because the former ions are larger, resulting in a longer metal−imidazole bond distance, weaker electrostatic interaction, and a proportionally smaller enhancement upon s−p hybridization.

s,d Orbital Occupation. Because the ionic radius of the metal decreases from left to right across the periodic table, the electrostatic contribution to bonding also increases. Therefore, the late transition metal ions generally bind more strongly than the early metal ions, as can be seen in Figure 6. Also obvious in the figure is the significant role that the s,d orbital occupation plays. All of the first row transition metal ions bind imidazole much more strongly than K^+ and Ca^+, the $4s^0$ and $4s^1$ ions of the same periodic row. However, strong variations in the binding across the first row indicate that the binding is influenced by other factors. Such variations have previously been explained for other metal−ligand complexes by examining the electron configuration of each of the metal ions.[4,14,18,20] These other factors arise as a result of the mechanisms by which the transition metal ion is capable of decreasing Pauli repulsion between the metal and the ligand. These mechanisms include 4s−4p hybridization, 4s−3dσ hybridization,[56,57] and promotion to a more favorable electronic state. Because the 4p orbitals lie higher in energy than the 3d orbitals, 4s−4p hybridization is more energetic than 4s−3dσ hybridization. 4s−4p hybridization is analogous to the mechanism observed in the Mg^+, Al^+, and Ca^+ systems in that it polarizes electron density to the opposite side of the metal ion, away from the ligand, allowing the ligand to experience a larger effective nuclear charge. 4s−3dσ hybridization also hybridizes electron density away from the ligand, but requires less energy and places electron density in a direction perpendicular to the bonding axis. When 4s−3dσ hybridization occurs, the transition metal center exists in a combination of low-spin states having $4s^13d^n$ and $3d^{n+1}$ configurations. Therefore, the promotion energy to the higher lying of these two states must be considered regardless of which of these corresponds to the ground state of the metal ion.

Pauli repulsion may also be reduced by promotion to an electronically excited state. In the discussion above, 4s−3dσ hybridization involves $3d^{n+1}$ and $4s^13d^n$ states of the same spin. The thermodynamic consequences of changing spin state to optimize metal−ligand bonding can also be observed, particularly when 4s−3dσ hybridization is not possible (e.g., when $n \geq 5$, there are no $3d^{n+1}$ states of the same spin as high-spin coupled $4s^13d^n$ states). In such cases, promotion to a state of lower spin must occur before 4s−3dσ hybridization can occur. Such promotion becomes more likely as the strength of the ligand field increases. This generally occurs as a result of interactions with multiple ligands, which are not examined here, although imidazole is a stronger field ligand than all of the ligands previously examined except adenine.

The early transition metal ions, Sc^+, Ti^+, and V^+, bind to imidazole and activate covalent bonds such that the BDEs for complexes of these metal ions to imidazole could not be directly measured. However, upper and lower bounds for the BDEs of these complexes were determined and should represent accurate limiting values as long as the M^+(imidazole) complexes accessed in our experiments did not involve inserted species. As a result, the following discussion for Sc^+, Ti^+, and V^+ will be based upon the theoretical trends. However, it should be noted that the upper and lower bounds for Sc^+ span the calculated value, while those for Ti^+ and V^+ are lower than but parallel to the calculated values. The ground-state electron configuration of Sc^+ is a triplet $4s^13d^1$; promotion to the triplet $3d^2$ configuration empties the 4s orbital decreasing the Pauli repulsion, but requires 57.5 kJ/mol.[58] The calculated M^+−N bond distance, 2.213 Å (Table 3S), is the largest of all of the transition metal ion−imidazole complexes studied. For Ti^+, the BDE is comparable, while the M^+−N bond distance is somewhat shorter, 2.118 Å. Ti^+ has two low-lying ^4F states, a $4s^13d^2$ ground state and a $3d^3$ exited state lying only 10.9 kJ/mol higher in energy.[58] These two states can mix to hybridize the 4s and 3dσ orbital, creating an empty acceptor orbital. This could increase the bonding slightly at the cost of hybridization, apparently resulting in a shorter but comparably strong bond. In going from Ti^+ to V^+, the BDE increases by 11.0 kJ/mol. The ground-state electron configuration of V^+ is d^4, and, therefore, the 4s orbital is unoccupied. The BDE increases as a result of the decreased Pauli repulsion and smaller size of the metal ion as seen by the shorter M^+−N bond distance, 2.058 Å.

The theoretical BDE decreases from V^+ to Cr^+, while the measured Cr^+ BDE is somewhat lower than the calculated value.

The ground-state electron configuration of Cr^+ is d^5 (^6S). The decrease in the ionic radius would suggest that Cr^+ (M^+-N = 2.011 Å) would bind more strongly than V^+. However, occupation of the 3dσ orbital leads to an increase in the Pauli repulsion and consequently weaker binding to imidazole.

The measured Mn^+−imidazole BDE is the weakest of all of the first−row transition metal ions and in excellent agreement with the calculated value. The binding is weakest to Mn^+ because it experiences the greatest Pauli repulsion. The ground state of Mn^+ (^7S) has a very stable electron configuration of $4s^13d^5$, such that both the 4s and the 3dσ orbitals are occupied and high-spin coupled. Therefore, Mn^+ cannot undergo 4s−3dσ hybridization without promotion, which costs a minimum of 113.3 kJ/mol to access the lowest lying quintet electronic state, the ^5S ($4s^13d^5$) state.[58] The M^+-N bond length, 2.139 Å, is longer than for all of the transition metal ions, except Sc^+.

The interaction of imidazole with Fe^+ is stronger than that with Mn^+, but weaker than the other late transition metal ions. The ground state of Fe^+ is ^6D ($4s^13d^6$), such that the 4s orbital is not empty. However, Fe^+ has a ^4F (d^7) excited state that lies only 22.4 kJ/mol above the ground state. The ^4F state of Fe^+ should experience decreased Pauli repulsion with the imidazole ligand and can utilize 4s−3ds hybridization, leading to stronger binding. Indeed, our theoretical calculations find that the ^4F excited state binds imidazole more strongly by 25.9 kJ/mol (Table 2). However, the excellent agreement between theory and experiment for the ^6D ground state of Fe^+ suggests that this is the state accessed in our experiments.

The BDEs of imidazole to Co^+, Ni^+, and Cu^+ are quite strong. These metal ions have ground-state electron configurations of $3d^n$ (n = 8, 9, and 10, respectively), which allow for direct σ-donation of the nitrogen lone pair electron density into the empty 4s orbital. The 4s−3dσ hybridization and comparatively small size of these metal ions compensates for the repulsive effects caused by the occupation of the 3dσ orbital and leads to the very strong bonds to these metal ions. This is illustrated by the three shortest M^+-N bonds (1.873, 1.811, and 1.776 Å, respectively) among the various transition metal ion−imidazole complexes, Table 3S. Although theory and experiments are consistent, theory finds that Ni^+ binds the most strongly, whereas experiment finds that Cu^+ binds the most strongly. The theoretical trend makes the most sense in that the binding increases with decreasing size of the metal ion, except for Cu^+, which is just slightly weaker than to Ni^+ as a result of complete occupation of the 3dσ orbital. The relative BDEs for Cu^+ and Ni^+ differ very little in both cases; the reversal in the relative strength of binding to these metal ions from theory to experiment may arise from experimental error in these measurements.

The BDE decreases from Cu^+ to Zn^+. The electron configuration of Zn^+ is $4s^13d^{10}$. Occupation of the 4s orbital results in an increase in Pauli repulsion. The effect is smaller than that observed for Mn^+ as a result of the smaller size of Zn^+. This is demonstrated by the difference in M^+-N bond lengths given in Table 3S, 2.139 Å for Mn^+ versus 1.952 Å for Zn^+.

Comparison with Ammonia and Adenine. Figure 7 compares the present experimental results for imidazole to those obtained in earlier studies for the binding of metal ions to ammonia[4] and adenine.[18] The BDEs of ammonia and adenine show trends similar to that observed here for imidazole. In addition, it is clear that the strength of the binding to imidazole is nearly equal to or slightly weaker than that to adenine, both of which bind more strongly than ammonia. Simplistically, this is the result expected on the basis of the polarizabilities[25] and

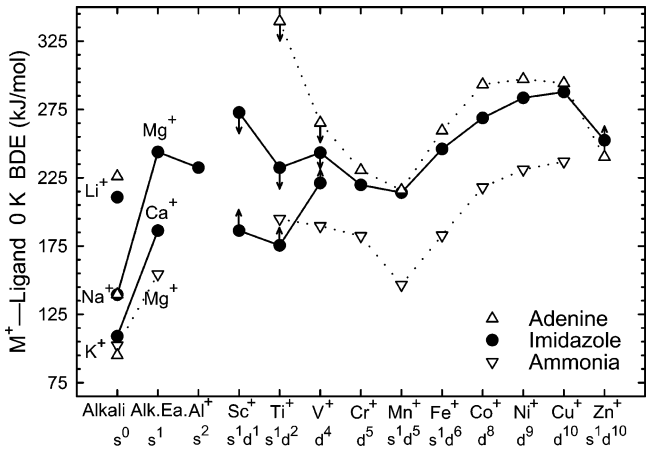

Figure 7. Periodic trends in experimental bond dissociation energies (in kJ/mol) for M^+-L, where L = adenine, imidazole, and ammonia. All values are at 0 K and are taken from Rodgers and Armentrout,[18] Table 2, and Walter and Armentrout,[4] respectively. Values shown with a downward point arrow represent upper bounds to the BDE, while those with an upward pointing arrow represent lower bounds to the BDE.

dipole moments of these ligands (13.1 Å^3 and 2.54 D for adenine[25,59] vs 7.17 Å^3 and 3.67 D for imidazole,[24,25,] and 2.16 Å^3 and 1.47 D for ammonia[25,60]). The adenine BDEs are 3 ± 6% larger than the imidazole BDEs. Thus, the effect of the 83% increase in the polarizability nearly cancels the 56% decrease in the dipole moment. The adenine and imidazole BDEs are only 33 ± 9% and 33 ± 13% larger than the ammonia values, respectively, even though their polarizabilities are 6.1 and 3.3 times larger than that of ammonia and the dipole moments are 1.7 and 2.7 times larger. Clearly, the BDEs are not linearly dependent on the polarizabilities or dipole moments. This indicates that the bond lengths probably vary and that other factors, such as chelation and binding conformation, are influential.

The preferred binding site for metal ions to adenine is at the N7 position of the imidazolic ring (analogous to the N3 position in imidazole) with additional stabilization provided by a chelation interaction with the amino group. In the neutral adenine molecule, the amino group is nearly planar and almost sp^2-hybridized to allow delocalization of the lone pair of electrons on the amino N atom with the aromatic π-electrons of the purine rings. The C6−NH_2 bond order of free adenine is generally regarded as 1.41−1.47.[61] Upon metal ion complexation at the N7 site, chelation with the amino group requires that it rotate out of the plane of the molecule and rehybridize to sp^3. This rehybridization is indicated by the H−N−H bond angle, which changes from 120.4° in neutral adenine to 103−104° in the M^+(adenine) complexes, and by the lengthening of the C6−NH_2 bond by ∼0.1 Å. The rotation and rehybridization of the amino group was theoretically estimated to require 55−70 kJ/mol in the absence of the metal ion.[13,18]

Comparison of the sum of the M^+−imidazole and M^+−ammonia BDEs minus the cost of resonance localization in the adenine molecule to the M^+−adenine BDEs shows that 75 ± 10% of the binding strength is recovered in the M^+(adenine) complexes for the complexes to Na^+, K^+, and V^+ through Cu^+. However, it might be more appropriate to replace the BDEs for binding of a second ammonia molecule rather than the first. This is because the sequential BDEs exhibit a monotonic decrease for nontransition metal ions, whereas the first and second BDEs to the transition metal ions are generally quite similar especially for small ligands where ligand−ligand repul-

sion is small. In this case, 75 ± 14% of the binding strength is recovered in the M^+(adenine) complexes. The largest values are obtained for Na^+ and K^+, the metal ions that do not benefit from 4s−3dσ hybridization, which is optimized for binding of two ligands directed 180° apart. This suggests that the inability to optimally coordinate to the N7 and NH_2 binding sites in adenine reduces the binding interaction by roughly 20−25%.

As discussed above, the BDEs for the early transition metal ions, Sc^+, Ti^+, and V^+, could not be accurately assessed as a result of the activated dissociation pathway leading to loss of HCN in the M^+(imidazole) complexes. However, it seems clear that the upper bounds to these values are closer to the true thermodynamic limits than the lower bounds as suggested by comparison with theory. In addition, the similar difference between the M^+(imidazole) and $M^+(NH_3)$ BDEs for Ti^+, V^+, and Cr^+ suggests that the upper limits cited in Table 2 for Ti^+ and V^+ are close to the true thermodynamic BDEs for these complexes. In contrast, the upper limit for the Sc^+ complex does not parallel the theoretical trend, and the activated dissociation product cross section exhibits two features, a small exothermic and large endothermic pathway, suggesting that the best estimate for the BDE of this complex may be the average of the upper and lower bounds given in Table 2.

Comparison with Glycine and Histidine. Relatively few measurements have been made for metal ion binding to the amino acids, particularly for histidine (His).[62,63,64,65] In addition, metal ion binding to isolated amino acids is dominated by the interactions with the backbone with additional stabilization provided by chelation interactions with the side chain. This contrasts the behavior in proteins where metal ions typically do not interact with the amino acid backbone, but instead bind to the side chains of several amino acids. As binding to the amino acid backbone generally involves interactions with both the carbonyl oxygen atom and the amino nitrogen atom, the interaction with the side chain represents the third binding site.[21] Comparison of the binding affinities of glycine (Gly) and His provides a measure of the enhancement in the binding as a result of the interaction with the imidizolic ring of the side chain of His. This interaction increases the binding affinity by 57 to 66 kJ/mol for Na^+,[64,] 56 kJ/mol for Cu^+,[62] and 75 kJ/mol for Ag^+.[63] The enhancement in the binding is similar for Na^+ and Cu^+ because the binding of more than two ligands to the transition metal ions eliminates the benefits that arise from 4s−3dσ hybridization in Cu^+. The enhancement in the binding for Ag^+ is larger because the larger size of this metal ion allows it to more effectively interact with all three groups without as significant of a loss in binding arising from steric effects. The enhancement in the binding to Na^+ and Cu^+ is significantly smaller than the corresponding M^+−imidazole BDEs measured here because the strength of metal−ligand interactions typically falls off monotonically with increasing extent of ligation. In addition, the identity of the metal ion becomes less important in determining the BDE as the extent of ligation increases. For example, the binding energy of the third acetonitrile molecule, that is, $(CH_3CN)_2M^+-(NCCH_3)$, is 88.8 ± 2.9 kJ/mol for Na^+ and slightly smaller for Cu^+, 84.1 ± 2.2 kJ/mol, and thus parallels the behavior in His.[22,23] This suggests that studies of the isolated models for the side chains of the amino acids may provide greater insight into the binding of metal ions in proteins than those involving the amino acids themselves.

Conclusions

The kinetic energy dependences of the collision-induced dissociation of M^+(imidazole), where $M^+ = Na^+$, Mg^+, Al^+, Ca^+, Sc^+, Ti^+, V^+, Cr^+, Mn^+, Fe^+, Co^+, Ni^+, Cu^+, and Zn^+, with Xe are examined in a guided ion beam mass spectrometer. The dominant dissociation process in most cases is loss of the intact imidazole ligand, although the Sc^+, Ti^+, and V^+ complexes show activated dissociation processes that compete with this channel. Thresholds for the simple CID processes are determined after consideration of the effects of reactant kinetic and internal energy distributions, multiple collisions with Xe, and lifetime effects. Insight into the structures and binding of the metal ions to the imidazole molecules is provided by theoretical calculations performed at the B3LYP/6-311+G(2d,2p)//B3LYP/6-31G* for the above 14 metal ions as well as to H^+, Li^+, and K^+. In addition, several additional levels of theory were examined for the computationally tractable systems: B3LYP/6-311++G(3df,3pd)//B3LYP/6-31G*, MP2(full)/6-311+G(2d,2p)//B3LYP/6-31G*, MP2(full)/6-311++G(3df,-3pd)//B3LYP/6-31G*, CBS-Q, and CBS-QB3. Although the calculated M^+−imidazole BDEs vary somewhat for each level of theory, all six levels of theory exhibit similar MADs as compared to the measured values. The excellent agreement between theory and experiment for the alkali metal ions, Li^+, Na^+, and K^+, as well as to the late transition metal ions Mn^+, Fe^+, Co^+, Ni^+, Cu^+, and Zn^+ suggest that the BDEs measured for these metal ions may be used as reliable anchors for the metal ion affinity scales. As relatively few measurements have been made for Mg^+, Ca^+, and Al^+, it is not clear that theory is able to describe these systems well. The activated dissociation pathways observed in the complexes to Sc^+, Ti^+, and V^+ do not allow absolute BDEs to be determined for these systems. However, the upper bounds reported here for Ti^+ and V^+ are likely very close to the true thermodynamic BDE for these complexes. The inability of each level of theory examined here to reliably provide accurate M^+−imidazole BDEs for all of the metal ions examined suggests that the imidazole molecule is not described well by theory and represents a good test case for the improvement of theoretical models, especially because imidazole is a building block of many important biological molecules.

Comparison of the M^+−imidazole BDEs to those of M^+−adenine complexes suggests that very little enhancement in the binding occurs because the loss of resonance delocalization caused by the rotation of the amino group out of the plane of the adenine molecule to allow chelation to the metal ion and the inability to optimally coordinate to the N7 and NH_2 binding sites in adenine nearly cancel the gain in binding. Clearly, this chelation interaction is important as significant repulsion between the metal ion and the amino group would exist if the amino group were to remain planar and not chelate to the metal ion and would result in much weaker binding than observed for adenine. In addition, the fact that metal ion binding in the isolated amino acids is dominated by interactions with the backbone, whereas only side-chain interactions are usually important in proteins, imidazole acts as a better model for metal ion binding to the His side chain in proteins than would studies of the isolated amino acid His.

Acknowledgment. This work was supported by the National Science Foundation, Grant No. 0138504.

Supporting Information Available: Tables of vibrational frequencies and average vibrational energies, rotational constants, B3LYP/6-31G* geometry optimized structures of imidazole and the M^+(imidazole) complexes, and thermal corrections, and figures showing cross sections for the collision-induced dissociation of the M^+(imidazole) complexes and

thermochemical analysis of the CID data. This material is available free of charge via the Internet at http://pubs.acs.org.

References and Notes

(1) Eichhorn, G. L. *Adv. Inorg. Biochem.* **1981**, *3*, 1.
(2) Eichhorn, G. L. In *Inorganic Biochemistry*; Eichhorn, G. L., Ed.; Elsevier: New York, 1973; p 1210.
(3) Rodgers, M. T.; Armentrout, P. B. *Mass Spectrom. Rev.* **2000**, *19*, 215.
(4) Walter, D.; Armentrout, P. B. *J. Am. Chem. Soc.* **1998**, *120*, 3176.
(5) Cowan, J. A. *Inorganic Biochemistry An Introduction*; VCH: New York, 1993.
(6) Rodgers, M. T.; Armentrout, P. B. *J. Phys. Chem. A* **1997**, *101*, 1238.
(7) Rodgers, M. T.; Armentrout, P. B. *J. Phys. Chem. A* **1997**, *101*, 2614.
(8) Rodgers, M. T.; Ervin, K. M.; Armentrout, P. B. *J. Chem. Phys.* **1997**, *106*, 4499.
(9) Rodgers, M. T.; Armentrout, P. B. *Int. J. Mass Spectrom.* **1999**, *185/186/187*, 359.
(10) Rodgers, M. T.; Armentrout, P. B. *J. Phys. Chem. A* **1999**, *103*, 4955.
(11) Armentrout, P. B.; Rodgers, M. T. *J. Phys. Chem. A* **2000**, *104*, 2238.
(12) Amunugama, R.; Rodgers, M. T. *Int. J. Mass Spectrom.* **2000**, *195/196*, 439.
(13) Rodgers, M. T.; Armentrout, P. B. *J. Am. Chem. Soc.* **2000**, *122*, 8548.
(14) Rodgers, M. T.; Stanley, J. R.; Amunugama, R. *J. Am. Chem. Soc* **2000**, *122*, 10969.
(15) Rodgers, M. T.; Armentrout, P. B. *J. Chem. Phys.* **1998**, *109*, 1787.
(16) Rodgers, M. T. *J. Phys. Chem. A* **2001**, *105*, 2374.
(17) Rodgers, M. T. *J. Phys. Chem. A* **2001**, *105*, 8145.
(18) Rodgers, M. T.; Armentrout, P. B. *J. Am. Chem. Soc.* **2002**, *124*, 2678.
(19) Huang, H.; Rodgers, M. T. *J. Phys. Chem. A* **2002**, *106*, 4277.
(20) Amunugama, R.; Rodgers, M. T. *J. Phys. Chem. A* **2001**, *105*, 9883.
(21) Ruan, C.; Rodgers, M. T. *J. Am. Chem. Soc.*, submitted for publication.
(22) Valina, A. B.; Amunugama, R.; Huang, H.; Rodgers, M. T. *J. Phys. Chem. A* **2001**, *105*, 11057.
(23) Vitale, G.; Valina, A. B.; Huang, H.; Amunugama, R.; Rodgers, M. T. *J. Phys. Chem. A* **2001**, *105*, 11351.
(24) Christen, D.; Griffiths, J. H.; Sheridan, J. *Z. Naturforsch.* **1982**, *37a*, 1378.
(25) Miller, K. J. *J. Am. Chem. Soc.* **1990**, *112*, 8533.
(26) Teloy, E.; Gerlich, D. *Chem. Phys.* **1974**, *4*, 417−427. Gerlich, D. *Inhomogeneous RF Fields: A Versatile Tool for the Study of Processes with Slow Ions Diplomarbeit*; University of Freiburg: Federal Republic of Germany, 1971. Gerlich, D. In *State-Selected and State-to-State Ion−Molecule Reaction Dynamics, Part I, Experiment*; Ng, C.-Y., Baer, M., Eds.; Advances in Chemical Physics Series; Wiley: New York, 1992; Vol. 82, p 1.
(27) Dalleska, N. F.; Honma, K.; Armentrout, P. B. *J. Am. Chem. Soc.* **1993**, *115*, 12125.
(28) Aristov, N.; Armentrout, P. B. *J. Phys. Chem.* **1986**, *90*, 5135.
(29) Hales, D. A.; Armentrout, P. B. *J. Cluster Sci.* **1990**, *1*, 127.
(30) Ervin, K. M.; Armentrout, P. B. *J. Chem. Phys.* **1985**, *83*, 166.
(31) Dalleska, N. F.; Honma, K.; Sunderlin, L. S.; Armentrout, P. B. *J. Am. Chem. Soc.* **1994**, *116*, 3519.
(32) Muntean, F.; Armentrout, P. B. *J. Chem. Phys.* **2001**, *115*, 1213.
(33) Beyer, T. S.; Swinehart, D. F. *Comm. Assoc. Comput. Machines* **1973**, *16*, 379. Stein, S. E.; Rabinovitch, B. S. *J. Chem. Phys.* **1973**, *58*, 2438−2445; *Chem. Phys. Lett.* **1977**, *49*, 183.
(34) Pople, J. A.; Schlegel, H. B.; Raghavachari, K.; DeFrees, D. J.; Binkley, J. F.; Frisch, M. J.; Whitesides, R. F.; Hout, R. F.; Hehre, W. J. *Int. J. Quantum Chem. Symp.* **1981**, *15*, 269. DeFrees, D. J.; McLean, A. D. *J. Chem. Phys.* **1985**, *82*, 333.
(35) Khan, F. A.; Clemmer, D. C.; Schultz, R. H.; Armentrout, P. B. *J. Phys. Chem.* **1993**, *97*, 7978.
(36) Chesnavich, W. J.; Bowers, M. T. *J. Phys. Chem.* **1979**, *83*, 900.
(37) See, for example, Figure 1 in: Dalleska, N. F.; Honma, K.; Armentrout, P. B. *J. Am. Chem. Soc.* **1993**, *115*, 12125.
(38) Armentrout, P. B.; Simons, J. *J. Am. Chem. Soc.* **1992**, *114*, 8627.
(39) Frisch, M. J.; Trucks, G. W.; Schlegel, H. B.; Scuseria, G. E.; Robb, M. A.; Cheeseman, J. R.; Zakrzewski, V. G.; Montgomery, J. A., Jr.; Stratmann, R. E.; Burant, J. C.; Dapprich, S.; Millam, J. M.; Daniels, A. D.; Kudin, K. N.; Strain, M. C.; Farkas, O.; Tomasi, J.; Barone, V.; Cossi, M.; Cammi, R.; Mennucci, B.; Pomelli, C.; Adamo, C.; Clifford, S.; Ochterski, J.; Petersson, G. A.; Ayala, P. Y.; Cui, Q.; Morokuma, K.; Malick, D. K.; Rabuck, A. D.; Raghavachari, K.; Foresman, J. B.; Cioslowski, J.; Ortiz, J. V.; Stefanov, B. B.; Liu, G.; Liashenko, A.; Piskorz, P.; Komaromi, I.; Gomperts, R.; Martin, R. L.; Fox, D. J.; Keith, T.; Al-Laham, M. A.; Peng, C. Y.; Nanayakkara, A.; Gonzalez, C.; Challacombe, M.; Gill, P. M. W.; Johnson, B.; Chen, W.; Wong, M. W.; Andres, J. L.; Gonzales, C.; Head-Gordon, M.; Replogle, E. S.; Pople, J. A. *Gaussian 98*, revision A.11; Gaussian, Inc.: Pittsburgh, PA, 1998.
(40) Becke, A. D. *J. Chem. Phys.* **1993**, *98*, 5648.
(41) Lee, C.; Yang, W.; Parr, R. G. *Phys. Rev. B* **1988**, *37*, 785.
(42) Foresman, J. B.; Frisch, *Æ Exploring Chemistry with Electronic Structure Methods*, 2nd ed.; Gaussian: Pittsburgh, 1996.
(43) Boys, S. F.; Bernardi, R. *Mol. Phys.* **1979**, *19*, 553.
(44) van Duijneveldt, F. B.; van Duijneveldt-van de Rijdt, J. G. C. M.; van Lenthe, J. H. *Chem. Rev.* **1994**, *94*, 1873.
(45) Moore, C. E. National Bureau of Standards, NSRDS-NBS-35; 1971; Vol. I, p 1.
(46) Main-Bobo, J.; Loesik, S.; Gase, W.; Baer, T.; Mommers, A.; Holmes, J. *J. Am. Chem. Soc.* **1986**, *108*, 677.
(47) Cradock, S.; Findlay, R. H.; Palmer, M. H. *Tetrahedron* **1973**, *29*, 2173.
(48) Ramsey, B. G. *J. Org. Chem.* **1979**, *44*, 2093.
(49) Klebe, K. J.; Houte, J. J. V.; Thuijl, J. V. *Org. Mass Spectrom.* **1972**, *6*, 1363.
(50) Lifshitz, C. *Adv. Mass Spectrom.* **1989**, *11*, 113.
(51) Bartlett, R. J. *Annu. Rev. Phys. Chem.* **1981**, *32*, 359.
(52) Hehre, W. J.; Radom, L.; Schleyer, P. v. R.; Pople, J. A. *Ab Initio Molecular Orbital Theory*; Wiley: New York, 1986.
(53) Hunter, E. P.; Lias, S. G. Proton Affinity Evaluation. In *NIST Chemistry WebBook*; NIST Standard Reference Database No. 69; Mallard, W. G., Lindstrom, P. J., Eds.; National Institute of Standards and Technology: Gaithersburg, MD, November, 1998; p 20899 (http://webbook.nist.gov).
(54) Burk, P.; Koppel, I. A.; Koppel, I.; Kurg, R.; Gal, J.-F.; Maria, P.-C.; Herreros, M.; Notario, R.; Abboud, J.-L. M.; Anvia, F.; Taft, R. W. *J. Phys. Chem. A* **2000**, *104*, 2824.
(55) Bauschlicher, C. W.; Partridge, H. *J. Phys. Chem.* **1991**, *95*, 9694.
(56) Bauschlicher, C. W.; Sodupe, M.; Partridge, H. *J. Chem. Phys.* **1992**, *96*, 4453.
(57) Bauschlicher, C. W.; Langhoff, S. R.; Partridge, H. *J. Chem. Phys.* **1991**, *94*, 2068.
(58) Sugar, J.; Corliss, C. *J. Phys. Chem. Ref. Data* **1985**, *14*, Suppl. 2.
(59) Boulton, A. J.; McKillop, A. In *Comprehensive Heterocyclic Chemistry*; Katritzky, A. R., Rees, C. W., Eds.; Pergamon Press: Oxford, 1984; Vol. 2, p 7.
(60) Rothe, E. W.; Bernstein, R. B. *J. Chem. Phys.* **1959**, *31*, 1619.
(61) Saenger, W. *Principles of Nucleic Acid Structure*; Springer-Verlag: New York, 1984.
(62) Cerda, B. A.; Wesdemiotis, C. *J. Am. Chem. Soc.* **1995**, *117*, 9734.
(63) Lee, V. W.-M.; Li, H.; Lau, T.-C.; Guevremont, R.; Siu, K. W. M. *J. Am. Soc. Mass Spectrom.* **1998**, *9*, 760.
(64) Kish, M. M.; Ohanessian, G.; Wesdemiotis, C. *Int. J. Mass Spectrom.* **2003**, *227*, 509.
(65) Gapeev, A.; Dunbar, R. C. *Int. J. Mass Spectrom.* **2003**, *228*, 825.